Evaluating the Performance of the ProtoDUNE–SP Detector using Michel Electrons

Aidan Reynolds

University College

University of Oxford

A thesis submitted for the degree of

Doctor of Philosophy

Hilary 2020

Abstract

This thesis presents the results of a study of electromagnetic interactions in the ProtoDUNE–SP liquid argon time projection chamber (LArTPC) detector. The LArTPC detector technology provides high spatial resolution on the final states of neutrino interactions, allowing interaction modes to be distinguished based on the event topology. In order to perform high precision measurements of ν_e in LArTPC detectors, electrons must be identified and their energy accurately reconstructed. In this work EM activity is studied in the 10–50 MeV range using Michel electrons as a source with a well defined energy spectrum. The sensitivity, bias, and energy scale are studied and the implications for neutrino physics in the Deep Underground Neutrino Experiment are discussed.

Contents

List of Figures

Glossary

DUNE . . . . . Deep Underground Neutrino Experiment.

EM . . . . . Electromagnetic.

LArTPC . . . Liquid Argon Time Projection Chamber.

PMNS . . . . . Pontecorvo—Maki—Nakagawa—Sakata

MLP . . . . . Multi–layer Perceptron

1 Introduction

Since the discovery of neutrino flavour oscillations, which implies that neutrinos have mass, neutrino physics has enjoyed a period of rapid development. The field has begun to transition into an era of precision, with many of the parameters governing these oscillations having been well constrained. The fact that neutrinos have mass, and the success of the PMNS theory in describing neutrino oscillations, leads to a number of fundamental questions which have important implications in both particle physics and cosmology:

- What is the mechanism giving rise to neutrino mass?
- What is the absolute scale and ordering of the neutrino masses?
- Do neutrinos and anti–neutrinos oscillate differently, and would this help to explain the matter anti–matter asymmetry in the universe?

In addition to these questions from the neutrino physics community, the high resolution and large masses of modern neutrino detectors make them useful tools for both astronomy and astrophysics. 2017 has widely been considered as the dawn of multi–messenger astronomy, with a measurement of gravitational waves at LIGO being correlated with measurements of a neutron star merger from electromagnetic telescopes [1]. This measurement was shortly followed by a similar correlation but

in the neutrino sector between a high energy neutrino event in ICECUBE and a number of traditional telescopes [2]. Within our galaxy, neutrino detectors provide a unique opportunity to understand the underlying mechanisms in supernovae; in the case of such a supernova, the structure of the neutrino flux at earth provides a mechanism to measure effects in the early stages of the supernova burst which are inaccessible with electromagnetic measurements [3].

Each of these questions places unique constraints on the design of an appropriate neutrino detector. The discovery of a matter anti–matter asymmetry in neutrino oscillations can be answered by making precise measurements of neutrino oscillations. This requires reliably identifying the flavour and energy of neutrinos in order to measure the appearance and disappearance spectra associated with neutrinos produced in long baseline neutrino experiments. To identify the low energy electrons produced in supernova neutrino interactions, a detector with low thresholds and low backgrounds is required. The Deep Underground Neutrino Experiment (DUNE) aims to tackle these challenges by utilising the Liquid Argon Time Projection Chamber (LArTPC) technology, whose high spatial and calorimetric resolution allows for more accurate topological classification of neutrino interactions [4]. To achieve these goals, a significant programme of LArTPC research is ongoing with construction, reconstruction, and analysis methods all under development in a number of LArTPC based experiments [5–8].

This thesis presents an analysis of charged particle interactions in the ProtoDUNE–SP LArTPC detector. A hit classification algorithm is developed and a sample of Michel electrons is used to provide a measurement of electron energy bias for low energy electrons. The analysis described in this thesis uses data collected with the ProtoDUNE–SP detector between August and November 2018.

Michel electrons have an energy spectrum spanning 0–60 MeV; understanding electrons in this energy range is important as they are the same energy as those produced when neutrinos from supernova bursts interact. In a LArTPC at these energies, the energy deposition of electrons transitions between ionisation dominated and radiation dominated regimes making for a particularly complicated combined

event topology [9]. The work presented here details a reconstruction strategy based on augmenting hit identification from a convolution neural network with simple clustering to identify and reconstruct Michel electron events. Analysis of these Michel electron events in ProtoDUNE–SP data and simulation quantifies the energy scale and energy scale bias for low energy electrons in a surface level LArTPC detector; this measurement can provide valuable input to studies of supernova burst neutrinos in LArTPC detectors.

Chapter 2 provides a theoretical overview of neutrinos within the standard model. Interactions, oscillations, and production will be discussed summarising the current knowledge in the field, as well as open questions which will be studied in ongoing and upcoming experiments. The role of neutrinos in supernova bursts and the detection of such neutrinos in a LArTPC detector will be discussed in more detail.

The ProtoDUNE–SP experiment is described in chapter 3, including details of the beam line, detector, cosmic ray flux, and simulations. An overview of the LArTPC detection principle will be given with specific details of the ProtoDUNE–SP design. Some details of detector operations will be discussed, paying particular attention to the monitoring of the detector via the online data quality monitoring system.

Chapter 4 will cover details of electromagnetic energy loss in liquid argon. Electron and photon energy loss will be discussed as well as processes leading to electron-ion recombination. The impacts of these effects on electron reconstruction in liquid argon will be highlighted.

The main analysis of this thesis will be described in chapters 5 and 6. Details of a hit classification algorithm based on convolutional neural networks will be given and Michel electron reconstruction will be highlighted as an example use for the output of this algorithm. Michel electron production and energy loss in liquid argon will be discussed. This will be followed by details of the reconstruction strategy used in the Michel electron analysis. The reconstructed Michel electron spectrum will be compared between data and simulation, and the energy resolution and energy scale bias for low energy electrons in the ProtoDUNE–SP detector will be estimated.

Chapter 7 will analyse the implications of the results of the Michel electron analysis for supernova neutrino physics in the DUNE experiment; the impacts of energy scale bias on these analyses will be investigated, and the possible performance of DUNE assuming the measured bias will be discussed.

A summary of the results presented in this thesis will be given in chapter 8 along with a discussion of the implications of these results for neutrino physics in LArTPC detectors.

2
Neutrino Physics

.

Contents

Despite being the second most abundant particle in the universe, neutrinos are some of the most elusive. Postulated by Wolfgang Pauli in 1930 **??**, to explain the continuous energy distribution of electrons emitted in β-decays, it would be over 25 years before Cowen and Reines would detect neutrinos in the vicinity of a nuclear reactor **??**. Since then our understanding of neutrino physics has expanded, three unique neutrino flavours have been discovered, and the discovery of neutrino oscillations makes neutrinos the only fundamental particle capable of time dependent flavour changes. The theory explaining neutrino oscillations, the Pontecorvo–Maki–Nakagawa–Sakata (PMNS) theory, has become well established by experimental measurements and leads to the possibility of CP–violation in the leptonic sector, a prerequisite for many explanations of the observed matter antimatter–asymmetry of the modern universe.

This chapter will review our current understanding of neutrino physics and the role of neutrinos in the Standard Model (SM). Theoretical aspects of neutrino physics will be reviewed in section 2.2, with a more detailed discussion of the theory of neutrino oscillations in section 2.3. Section 2.4 will give details of neutrino interactions and production. The production of neutrinos in supernova bursts will be discussed in section 2.5, and the role of neutrinos in understanding supernovae will be highlighted.

2.1 A Brief History of Neutrino Physics

When the energy spectra of electrons in β–decays where first measured the results posed a problem. At the time the β–decay interaction was believed to lead to a two–body final state and, as such, the emitted electrons should be released with a single well defined energy. Therefore the observation of a broad spectrum of electron energies appeared to disobey conservation of energy, in 1930 Pauli proposed a solution to this problem by postulating an additional particle that was evading detection but sharing the released energy with the electron, thus preserving conservation of energy. Despite Pauli's belief that he had proposed the existence of something that "cannot be detected", in 1956 Cowen and Reines would announce that they had observed positrons produced by the inverse beta decays of neutrinos from a nuclear reactor.

After the first observation of neutrinos the progression in experimental neutrino physics became more rapid. TODO

2.2 Neutrinos in the Standard Model

In the Standard Model (SM) Neutrinos, and their interactions, are governed by the electroweak (EW) theory, a gauge theory on the SU(2) × U(1) group. In this theory, neutrinos transform along with charged leptons as part of the left handed fermion doublets

$$\Psi = \left\{ \begin{pmatrix} \nu_i \\ l_i^- \end{pmatrix}, \begin{pmatrix} u_i \\ d_i' \end{pmatrix} \right. \tag{2.1}$$

where $d_i' = \sum_j V_{ij} d_j$, and V is the Cabibbo-Kobayashi-Maskawa (CKM) mixing matrix.

2.3 Neutrino Oscillations

2.4 Neutrino Interactions

2.5 Supernova Neutrinos

3

The ProtoDUNE–SP Detector

Contents

This chapter will discuss the ProtoDUNE–SP experiment and it's role in the development of the proposed DUNE experiment. The LArTPC technology will be detailed in the general case and then the specifics of the ProtoDUNE–SP detector will be given. Details of the major particle fluxes in ProtoDUNE–SP will be outlined, along with a discussion of the simulation and reconstruction of each flux. Finally, as my main contribution to detector operations during data taking was developing for the ProtoDUNE–SP online monitoring system, this will be discussed in more depth.

The work for the online monitoring subsection has been completed as part of my duties as an on–site expert at CERN. I expect to be able to complete the rest of the work by the end of December 2019 alongside the other analysis work.

3.1 Liquid Argon Time Projection Chambers

3.2 The ProtoDUNE–SP LArTPC

3.3 The H4 Beam Line

3.4 Cosmic Rays in ProtoDUNE–SP

3.5 ProtoDUNE–SP Simulation and Reconstruction

3.6 The ProtoDUNE–SP Online Monitoring System

4

Energy Loss in Liquid Argon

Contents

This chapter will cover in more detail both the theory and measurement of electromagnetic energy loss in liquid argon. Energy loss for both electrons and photons will be discussed and the implications of this for electron reconstruction at different energy scales will be highlighted.

The work in this section is complete and part of this work was reported in the document submitted for transfer of status.

4.0.1 Electron Energy Loss

4.0.2 Photon Energy Loss

4.0.3 Electron–Ion Recombination

4.0.4 Implications on Electron Reconstruction in Liquid Argon

5

Charge Identification with Convolutional Neural Networks

Contents

A major problem faced by the next generation of neutrino experiments is the correct categorisation of particle interactions within the detector. Typically identifying the underlying type of a neutrino interaction involves determining the lepton content of the final state particles; as such it is important to be able to distinguish muons from electrons, or more generally tracks from showers.

This chapter will describe an approach for hit classification in LArTPCs using machine learning techniques. A brief theoretical overview of neural networks will be presented in section 5.1, including a discussion of convolutional neural networks and their application to pattern recognition. Section 5.2 will detail an approach to hit classification in LArTPCs based on tagging the source of energy depositions with a convolutional neural network. The performance of this approach will be analysed with ProtoDUNE–SP simulation and data in sections 5.3 and 5.4 respectively.

5.1 Neural Networks

An artificial neural network (ANN) consists of a set of nodes, together with a set of connections between those nodes. The nodes in the graph take the form of an artificial neuron which passes a number of inputs through a nonlinear activation function to produce a single output. In an ANN the connections provide a mechanism for taking the output of a given node and using it as the input for a subsequent node. This structure of nodes and connections provides a very flexible framework, the basis for a number of machine learning algorithms which utilise this flexibility to learn the structure of complex data sets.

In order for an ANN to make accurate predictions based on data, the weights and biases between each set of neurons must be tuned such that the outputs of the network match those expected for a given input. In supervised learning [10], the loss, a measure of the difference between the truth and the output of an ANN, can be used to learn the appropriate values of the weights and biases using the method of gradient descent. The loss is computed and its gradient as a function of the weights and biases can be calculated with the back–propagation algorithm [11]; the loss is then minimised based on the gradient calculated with back–propagation. This process can be repeated until the loss function reaches an acceptable level or stops decreasing.

One of the most widely used ANN's is the multi–layer perceptron (MLP) [10]; this class of networks consists of at least three layers of nodes: an input layer, one or more hidden layers, and an output layer. These layers are connected in a feed–forward configuration such that the graph of nodes contains no cycle. Traditionally, the layers are also fully connected such that the output of each node is connected to the inputs of all nodes in the next layer. These networks are able to approximate any function to arbitrary precision with a single hidden layer [12]; however, there is no limit on the number of nodes required in order to achieve a good approximation. In practice networks with additional hidden layers can reach the required precision with fewer nodes than a network with a single hidden layer [13].

ANN's provide a flexible tool for a variety of pattern recognition tasks but there can be issues with their training and use. Typical issues with ANN's include a risk of slow learning due to vanishing gradients for typical sigmoid activation functions and a high risk of over–training due to the large number of free parameters. In particular, over–training can lead to poor generalisation of the network for real world examples, despite excellent performance when evaluated on the training sample [10].

An extension of the MLP with considerable success, particularly in image classification tasks, is the convolutional neural network (CNN) [14, 15]. When evaluating data with a high dimensional input, having a fully connected network architecture leads to large numbers of neurons and high computational cost. In addition, for spatially correlated data such an architecture does not take the local spatial structure of the data into account. A CNN attempts to resolve these issues by exploiting the local connectivity of the data; single input neurons are replaced by convolutional kernels which are evaluated on small regions of the input. These convolutional kernels are evaluated over all valid locations in the input producing feature maps which describe the spatial distribution of the features which each kernel has learned to identify. Each set of feature maps can then be used as an input for either convolutional layers or fully connected layers.

Convolutional kernels provide a local translation invariant evaluation of features within the data; with this method low level features are identified first and their spatial distribution can then be exploited to identify higher level structure in the data [14]. This makes these networks ideal for pattern recognition in images, where common features can be located anywhere in the image. The high spatial and calorimetric energy resolution of LArTPC detector data make these algorithms an ideal candidate for classification of the data, and successful applications on CNNs have been achieved in ongoing neutrino experiments [16, 17]. The remainder of this chapter will detail a use of CNNs to identify low level features in LArTPC data.

5.2 Hit Identification with Convolutional Neural Networks

As well as in neutrino event classification, effective track shower separation has important applications throughout DUNE's physics programme; defining pure calibration samples such as minimum ionising muons and π_0 decays is crucial for understanding the energy response of the DUNE detector. Each of these samples has a unique topology, but the first step in identifying many of these samples is the same: defining tracks and showers which can be combined to give the final state. To do this collections of hits have to be clustered and identified as track or shower objects. Here we will present a method for classifying the ionisation source of hits, a label is then associated with each hit, and subsequent reconstruction and analysis algorithms can use this when defining data samples.

Aside from track and shower objects, a useful calibration sample with a unique topology in LAr is the Michel electron. At typical Michel electron energies the ionisation energy loss of electrons in LAr undergoes a transition from collision dominated to radiation dominated, as such Michel electrons typically have a combined topology with a short track–like component and a few small radiated energy depositions. Due to the unique topology of these interactions, Michel electrons where chosen as a unique category for hit classification.

A CNN was used for hit classification, the network was trained to predict $\{p_t, p_s, p_e, p_m\}$, the probabilities for track, shower, empty, and Michel classifications respectively. The empty category is included to ensure that the network doesn't learn to assign a track–like or shower–like tag to empty or noisy regions of the data. Since the Michel electron category has overlap with the track and shower categories, the Michel electron probability is decoupled from the other probabilities which are constrained to sum to one.

Training data was built using simulations of the ProtoDUNE–SP detector in the LArSoft framework [18]; cosmic ray simulations were combined with simulations of the ProtoDUNE–SP beam for peak beam energies in the range 1–7 GeV and both positive and negative beam polarity. The input was formed of small patches of the

raw detector readout in each plane, 48 wires in total where considered around the central energy deposition and an equal number of bins were formed in the drift time coordinate by averaging the ADC values over time such that the distance scale was equal in both coordinates. The truth for each training sample was obtained from the simulation by associating the measured ionisation energy depositions to the corresponding simulated particle. In total $\sim$ 26 million input patches were produced, figure 5.1 shows example patches for each label type, and details of the number of each patch type in the training, validation, and test data sets are given in table 5.1.

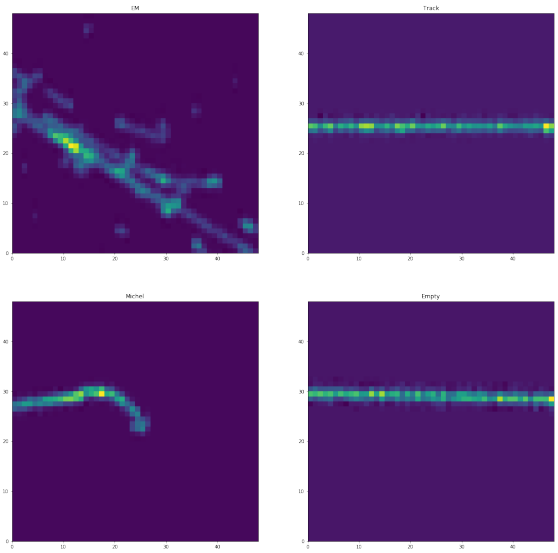

Figure 5.1: Example input patches for each label. Clockwise from top–left: Shower, Track, Empty, Michel.

Patch Type	Shower	Track	Empty	Michel
Training	13,493,982	9,727,604	2,517,882	731,456
Validation	734,673	562,038	141,388	42,727
Test	764,659	518,805	139,987	39,674

Table 5.1: Summary of the number of samples with each truth label in the training, test, and validation data sets.

The network architecture was designed to provide the best performance possible given constraints on running time; since the CNN is part of the low level reconstruction chain and it must run over a large number of candidate images for each event, run time for each event is required to be $O(10)$s. While better

classification performance was achieved with deeper networks, the best performance while achieving the running time goal was achieved with a relatively shallow network consisting of one convolutional layer followed by two dense layers; it is reasonable to assume that with improved computational resources, e.g. evaluation with GPU's, the performance of the classification could be improved within the time constraints.

The TensorFlow library was used to design and train the CNN, with the TensorBoard visualisation suite being used to monitor training [19]. The final network architecture used is shown in figure 5.2; the 48×48 pixel input images are passed through a single convolutional layer with 48 5×5 filters; the output feature map is passed onto a pair of dense layers with 128, and 32 nodes respectively. Leaky rectified linear units are used as activation functions throughout the hidden layers [20]. These units are more computationally efficient than sigmoid like functions as well as providing a non–vanishing gradient for all inputs, avoiding saturation in learning. The output of the network is split into two branches; a three–way softmax function is used to constrain the joint probability for track, shower, and empty to sum to one, and a sigmoid function is used for the output of the Michel electron classifier. Finally, regularisation is achieved with the dropout algorithm [21]; in each iteration of the training weights have a probability p to be set to zero while the remaining weights are scaled by a factor $1/(1-p)$. With this approach, each training iteration uses only a random sample of the available nodes and as such nodes cannot co–adapt. The resulting network is a model average of each possible sub–network.

The network was trained using stochastic gradient descent (SGD) with the total loss being the weighted sum of the losses for the two output branches, $L_{tot} = 0.1 \cdot L_{tse} + L_m$, where the Michel classifier is given higher precedence due to the smaller training data set available for the Michel output. In order to speed up the learning process and converge on an optimal model, both the momentum and decay algorithms were used; momentum reduces oscillations of the weights during learning, while the decay of the learning rate allows for rapid learning during early stages of SGD and increased precision as the model converges [10]. Learning metrics were monitored during training using TensorBoard. The losses for each

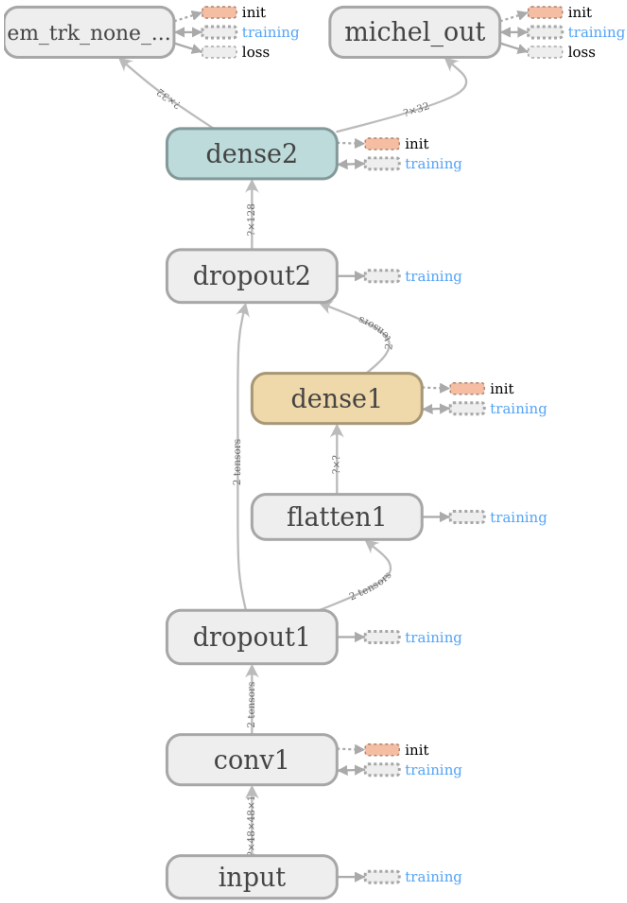

Figure 5.2: Network architecture used for hit classification, visualisation from the TensorBoard library.

branch as well as the total loss for the validation data set are given in figure 5.3 as a function of the training epoch. The validation losses remain stable giving an indication that regularisation with dropout was successful in preventing over–fitting of the training data. However, the validation set loss does not increase significantly after the first couple of epochs and so the training could have been terminated sooner with this network architecture. The final losses measured with the test data set are given in table 5.2.

Loss Type	L_{tot}	L_{tse}	L_m
Loss Value	0.033	0.155	0.017

Table 5.2: Test set losses after full training process.

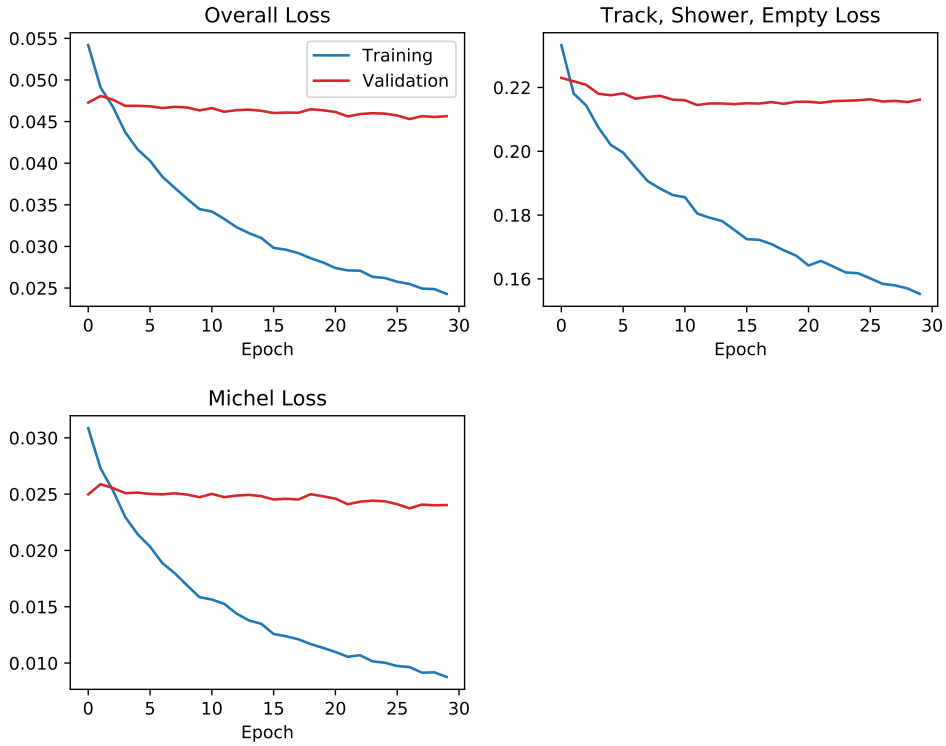

Figure 5.3: Evolution of the validation and training set losses during the training process.

5.3 Performance on ProtoDUNE–SP Simulation

The performance of the hit tagging was evaluated with reconstructed events in the ProtoDUNE–SP detector from the latest simulation samples; in the simulations, the detector was simulated under a number of different conditions, specifically including the space charge effect (SCE) [22] and excluding it. The hit tagging was trained on a part of the simulated data set which included the SCE and, as such, the samples without the SCE can be used as a validation that the network is robust to SCE differences between the simulations, and hence between the simulations and the data.

The distributions of the shower like classifier output for true shower hits and all other hits are given in figure 5.4; a strong separation between track and shower hits is observed. The shower classification threshold was optimised based on the F1 metric. This metric is defined as the harmonic mean of the precision and recall of a classifier and optimising with this score will ensure that both precision and recall will be high in the final classifier; for use cases where neither precision or recall is

favoured, the F1 metric can be used to optimise for the best overall performance. The value of the F1 metric as a function of threshold is also shown in figure 5.4; the score peaks at a threshold of 0.72 with a value of 0.863 corresponding to a precision of 0.863 and a recall of 0.863.

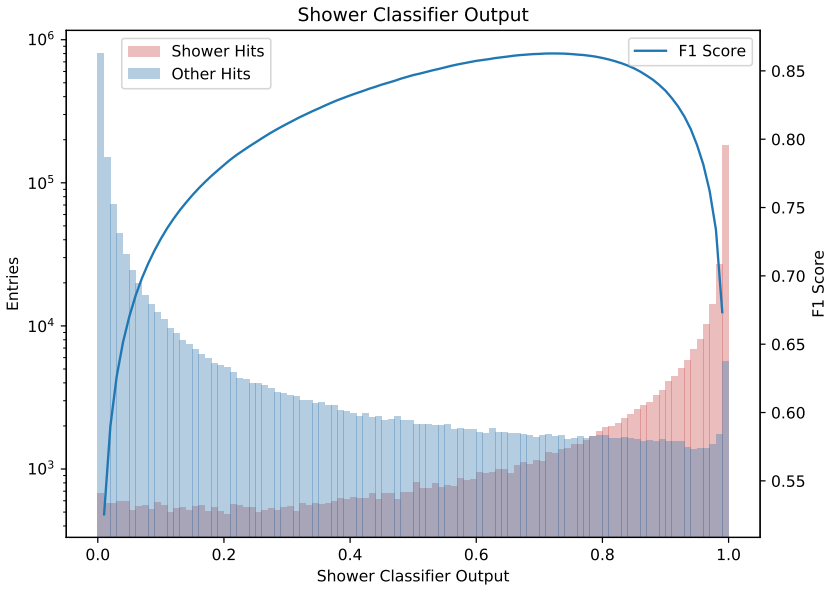

Figure 5.4: Shower classifier output distributions for true showers, and all other hits. Threshold optimisation was done using the F1 score metric which is also plotted.

Figure 5.5 gives the distributions of the Michel classifier output for true Michel electrons and all other hits. The large difference in sample size between the Michel electron and other hits in this sample means that despite high recall by the Michel electron classifier, low precision is achieved. In chapter 6 we will see that despite the low performance of the classifier for individual hits, a pure sample of Michel electron events can be selected by clustering hits with high Michel electron scores. This is due to the fact that the simple hit by hit classification test does not account for spatial correlations between Michel tagged hits.

Finally, the overall performance of each classifier was evaluated using the receiver operating characteristic (ROC) curve [23]; ROC curves are a test of the classification ability of a binary classifier. The curves show a comparison of the true positive rate and the false positive rate of the classifier as a function of the classification

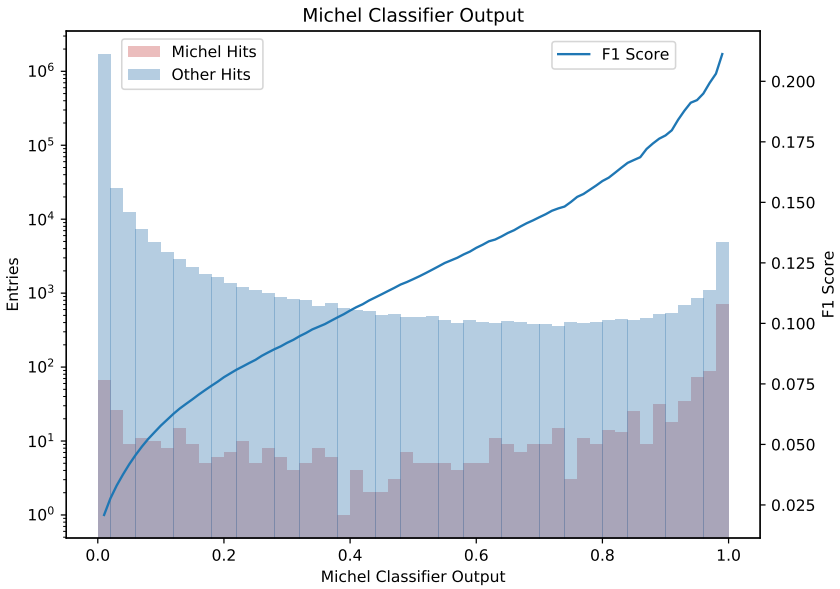

Figure 5.5: Michel classifier output distributions for true Michel electrons, and all other hits. Threshold optimisation was initially done with the F1 score metric, the threshold was modified when combined with a clustering algorithm, see chapter 6.

threshold chosen for the classifier. Figure 5.6 shows the ROC curves for the shower and Michel classifiers; the locations of these curves in the top left corner of the plots show that both have excellent performance as classifiers. In addition, the ROC curves show good agreement between the SCE on and SCE off data sets, showing that the classifiers are robust to changes in the SCE model should it differ between data and simulation. It is worth noting that the ROC curve only accounts for classification rates within each true sub–sample, it cannot account for the difference in sample size between the Michel electron sample and all other hits, and thus the ROC curve is a more instructive metric for the shower classifier where the size of the true and false samples are of a similar magnitude.

5.4 Validation and Performance on ProtoDUNE–SP Data

For validation on real ProtoDUNE–SP data two approaches were used: visual validation with event scans and cross validation with the output of the Pandora reconstruction framework [24]. Data from ProtoDUNE–SP run number 5387 was

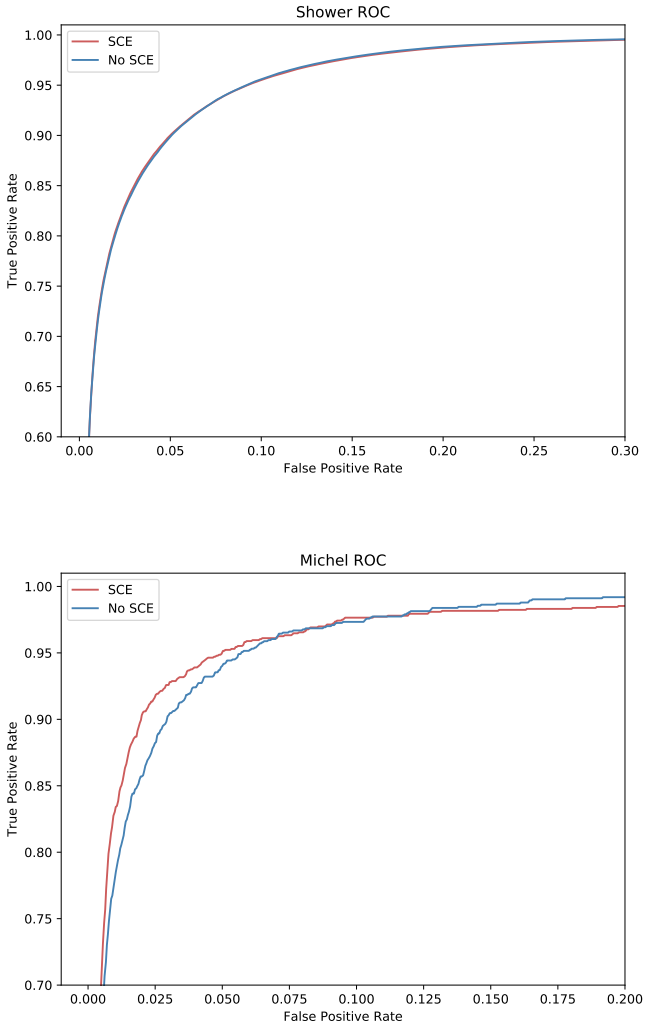

Figure 5.6: ROC curves for the shower (top), and Michel (bottom) classifiers. ROC curves for simulations including and excluding the SCE are included.

used for the validation; the data for this run was taken under stable operating conditions with a peak beam energy of 1 GeV.

Hand scans of the events show qualitatively that performance on the data is good. Figure 5.7 shows an example of the track like classification of hits in a real event. We can see that for hits along the tracks the classifier produces a large output score, and for shower like activity in the event the score is low, as we expect. In particular the classifier is able to identify that hits which are adjacent to the track, delta rays, are from scattered electrons.

The Pandora reconstruction framework is the primary reconstruction used by the

ProtoDUNE–SP experiment; for a more quantitative validation of the performance of the hit tagging algorithm, the hit tagging output can be compared to the reconstructed objects produced by Pandora. After the ProtoDUNE–SP data has been reconstructed, all of the reconstructed hits will have been clustered into either track or shower objects. As such the comparison of a hits CNN output with the type of reconstructed object it belongs to is a test of the agreement between the CNN approach and the Pandora reconstruction algorithms. The Michel electron performance cannot be validated in this way due to a lack of tagged Michel electron objects in the Pandora output. Therefore, hand scanning of events is the primary validation of the Michel electron classifier and will be discussed in chapter 6.

The first test performed was the comparison of the CNN output distributions for hits in both Pandora tracks and Pandora showers, the corresponding distributions are given in figure 5.8 for both data and Monte Carlo; a strong correlation between the reconstructed Pandora objects and the associated CNN score can be seen in both cases, however the correlation is stronger in Monte Carlo than in data. The discrepancy between Pandora and the CNN is still being understood, differences between the data and simulations impact the performance of both algorithms. Figure 5.7 shows reconstructed hits labelled according to whether they agree or disagree with Pandora, we can see that for long tracks the agreement is good while smaller objects tend to disagree, with the CNN typically assigning a shower like classification but Pandora reconstructing them as a track. Work to understand the discrepancy between the CNN score and Pandora is ongoing.

This chapter has presented work on the development of a hit classification algorithm for LArTPCs based on CNNs; the performance of this approach for track–shower separation has been evaluated with ProtoDUNE–SP simulation and reconstruction, demonstrating good performance. This hit tagging framework is designed such that it can be utilised throughout the LArSoft reconstruction chain and is complementary to other reconstruction algorithms in the framework; chapter 6 will detail an example use of the hit tagging output: Michel electron event selection. Additional plans for this chapter are detailed below.

- Understand the difference between data and MC when comparing the CNN to Pandora.
- Test network robustness to other detector effects in simulation.
- Retrain networks with future simulations, including data driven models of detector effects.

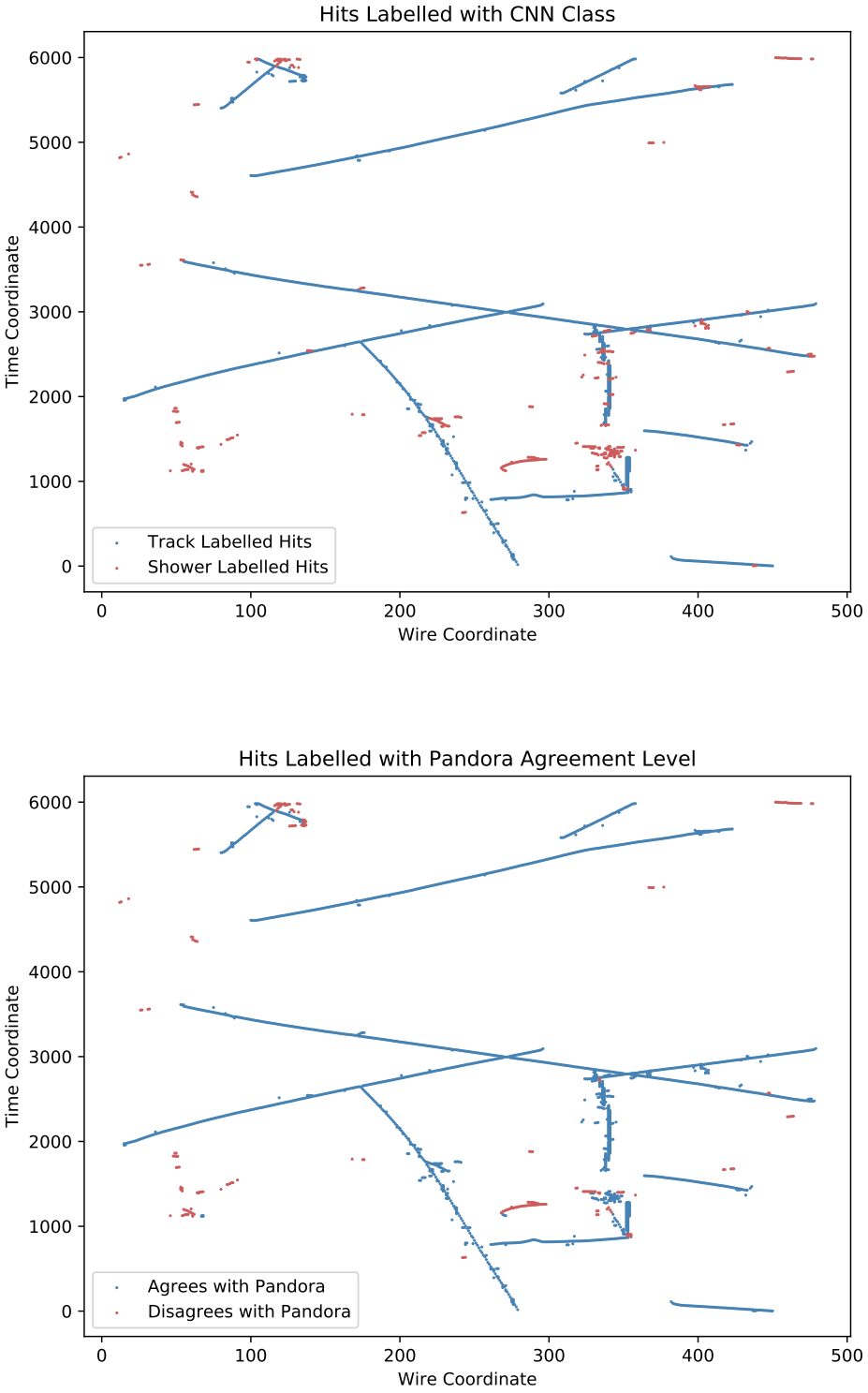

Figure 5.7: Reconstructed hits from ProtoDUNE–SP run number 5387 labelled with CNN classification (top), and Pandora agreement level (bottom).

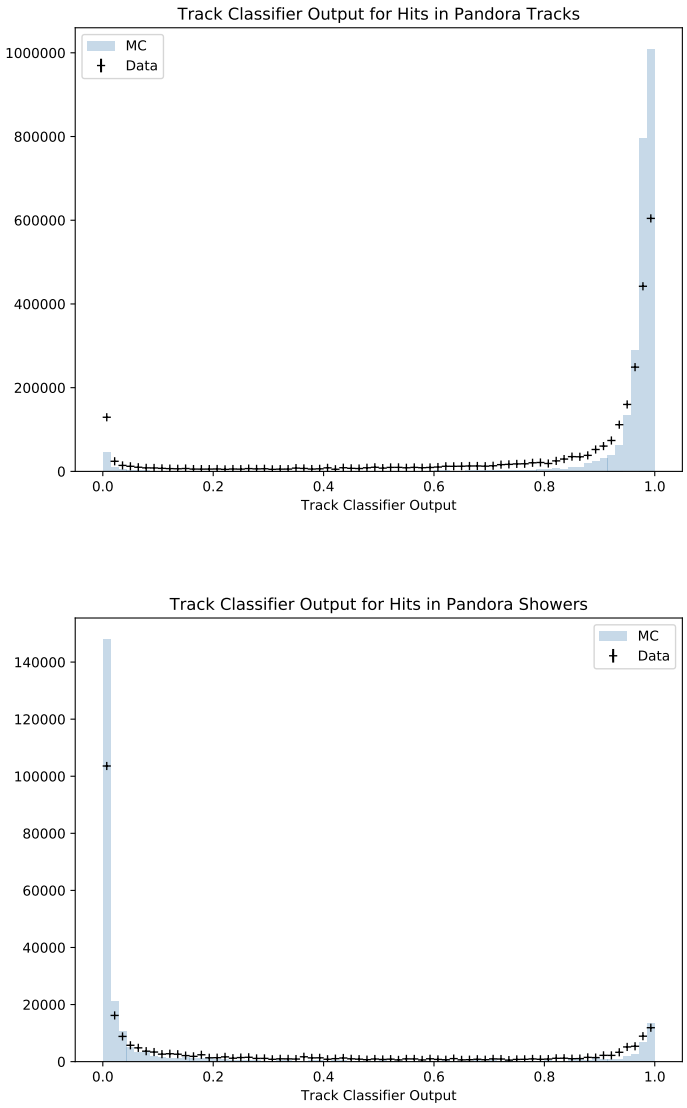

Figure 5.8: Output distributions for the track classifier on reconstructed Pandora objects.

6

Study of Michel Electrons in ProtoDUNE–SP

Contents

This chapter will cover the primary analysis of this thesis; a study of Michel electrons in the ProtoDUNE–SP detector which aims to investigate the agreement between data and simulation, and to provide an estimate of the energy scale uncertainty and energy scale bias for electrons in the 0–60 MeV range.

The work done for this section is ongoing; preliminary work on this topic was presented in the report submitted for transfer of status. The rest of the work for this section is expected to be completed by the end of October 2019.

The work done as of writing for this chapter is as follows:

- Event selection algorithm developed based on clustering of the Michel like hits discussed in the previous chapter.

  - Purity of $> 98\%$ and efficiency of 5% measured in ProtoDUNE–SP simulations.

- Two possible energy reconstruction algorithms developed.
  - Cone algorithm.
  - Semantic segmentation algorithm with U-ResNet CNN architecture.

The work left to do is as follows:

- Validation of algorithms on the real ProtoDUNE–SP data.
- Data MC comparison for Michel electron energy spectrum.
- Energy scale uncertainty and energy scale bias measurements with measured Michel electron energy spectrum.

An example Michel electron candidate event from the real ProtoDUNE–SP data is given in figure 6.1.

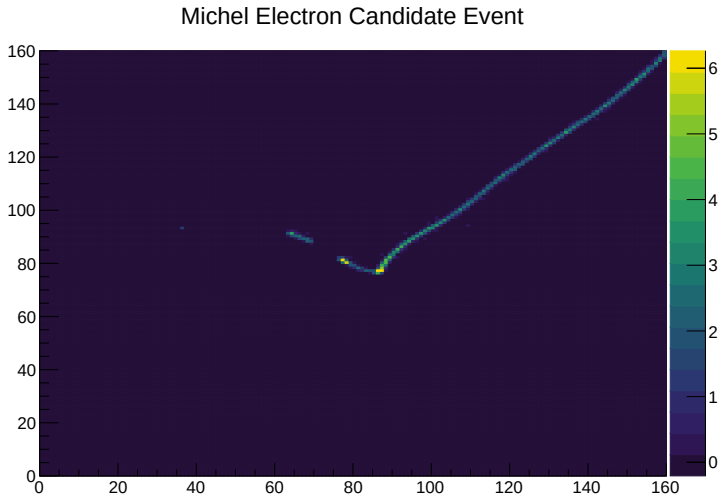

Figure 6.1: Michel electron candidate event from ProtoDUNE–SP data.

6.1 Michel Electrons in Liquid Argon

6.2 Electromagnetic Energy Loss in Liquid Argon at 0–60 MeV

6.3 Michel Electron Event Selection

6.4 Michel Electron Energy Reconstruction

6.5 Reconstructed Michel Electron Spectrum

7
Implications for DUNE

Contents

This chapter will analyse the implications of the measured uncertainties on analyses for the DUNE experiment. In particular the impact of the measured energy scale uncertainty and energy scale bias on supernova neutrino physics in DUNE will be analysed. The difference in conditions between ProtoDUNE–SP and DUNE will be highlighted and the expected implications for energy scale uncertainties in DUNE will be discussed.

The work for this section has yet to be started as it will be dependent on the outcome of the Michel electron analysis in the previous section. I expect to be able to start work on this analysis in September/October 2019 after preliminary results of the Michel electron analysis; work for this section will be completed by the end of December 2019.

7.1 Supernova Neutrinos in DUNE

7.2 Impacts of Energy Uncertainties

8
Conclusions

This chapter will summarise the work presented in the thesis and provide concluding remarks on the implications of the results for future analyses in LArTPC experiments.

References

[1] G. Vedovato et al. “GW170817: Observation of Gravitational Waves from a Binary Neutron Star Inspiral”. In: *Physical Review Letters* 119.16 (2017), pp. 30–33.

[2] M. G. Aartsen et al. “Multimessenger observations of a flaring blazar coincident with high-energy neutrino IceCube-170922A”. In: *Science* 361.6398 (2018). arXiv: 1807.08816.

[3] Kate Scholberg. “Supernova Neutrino Detection”. In: *Ann. Rev. Nucl. Part. Sci.* 62 (2012), pp. 81–103. arXiv: 1205.6003 [astro-ph.IM].

[4] R. Acciarri et al. “Long-Baseline Neutrino Facility (LBNF) and Deep Underground Neutrino Experiment (DUNE)”. In: (2016). arXiv: 1601.05471 [physics.ins-det].

[5] R. Acciarri et al. “Design and Construction of the MicroBooNE Detector”. In: *JINST* 12.02 (2017), P02017. arXiv: 1612.05824 [physics.ins-det].

[6] F. Cavanna et al. “LArIAT: Liquid Argon In A Testbeam”. In: (2014). arXiv: 1406.5560 [physics.ins-det].

[7] M. Antonello et al. “A Proposal for a Three Detector Short-Baseline Neutrino Oscillation Program in the Fermilab Booster Neutrino Beam”. In: (2015). arXiv: 1503.01520 [physics.ins-det].

[8] B. Abi et al. “The Single-Phase ProtoDUNE Technical Design Report”. In: (2017). arXiv: 1706.07081 [physics.ins-det].

[9] R. Acciarri et al. “Michel Electron Reconstruction Using Cosmic-Ray Data from the MicroBooNE LArTPC”. In: *JINST* 12.09 (2017), P09014. arXiv: 1704.02927 [physics.ins-det].

[10] Russell D. Reed and Robert J. Marks. *Neural Smithing: Supervised Learning in Feedforward Artificial Neural Networks*. Cambridge, MA, USA: MIT Press, 1998.

[11] David E Rumelhart, Geoffrey E Hinton, and Ronald J Williams. “Learning representations by back-propagating errors”. In: *Nature* 323.6088 (1986), pp. 533–536. URL: https://doi.org/10.1038/323533a0.

[12] George Cybenko. “Approximation by superpositions of a sigmoidal function”. In: *MCSS* 2 (1989), pp. 303–314.

[13] Yann Lecun, Yoshua Bengio, and Geoffrey Hinton. “Deep learning”. In: *Nature* 521.7553 (2015), pp. 436–444. arXiv: 1807.07987.

[14] L. D. Jackel et al. *Backpropagation Applied to Handwritten Zip Code Recognition*. 2008. arXiv: 1004.3732.

[15] Christian Szegedy et al. “Going deeper with convolutions”. In: *Proceedings of the IEEE Computer Society Conference on Computer Vision and Pattern Recognition*. 2015. arXiv: 1409.4842.

[16] A. Aurisano et al. "A Convolutional Neural Network Neutrino Event Classifier". In: *JINST* 11.09 (2016), P09001. arXiv: 1604.01444 [hep-ex].

[17] R. Acciarri et al. "Convolutional Neural Networks Applied to Neutrino Events in a Liquid Argon Time Projection Chamber". In: *JINST* 12.03 (2017), P03011. arXiv: 1611.05531 [physics.ins-det].

[18] E. L. Snider and G. Petrillo. "LArSoft: Toolkit for simulation, reconstruction and analysis of liquid argon TPC neutrino detectors". In: *Journal of Physics: Conference Series* 898.4 (2017).

[19] Martin Abadi et al. "TensorFlow: A system for large-scale machine learning". In: *12th USENIX Symposium on Operating Systems Design and Implementation (OSDI 16)*. 2016, pp. 265–283. URL: https://www.usenix.org/system/files/conference/osdi16/osdi16-abadi.pdf.

[20] Kaiming He et al. "Delving deep into rectifiers: Surpassing human-level performance on imagenet classification". In: *Proceedings of the IEEE International Conference on Computer Vision* (2015), pp. 1026–1034. arXiv: 1502.01852.

[21] Nitish Srivastava et al. "Dropout: a simple way to prevent neural networks from overfitting". In: *Journal of Machine Learning Research* 15 (2014), pp. 1929–1958.

[22] Michael Mooney. "The MicroBooNE Experiment and the Impact of Space Charge Effects". In: *Proceedings, Meeting of the APS Division of Particles and Fields (DPF 2015): Ann Arbor, Michigan, USA, 4-8 Aug 2015*. 2015. arXiv: 1511.01563 [physics.ins-det].

[23] Tom Fawcett. "An Introduction to ROC Analysis". In: *Pattern Recognition Letters* 27.8 (2006), pp. 861–874.

[24] J. S. Marshall and M. A. Thomson. "The Pandora software development kit for pattern recognition". In: *European Physical Journal C* 75.9 (2015), pp. 1–16. arXiv: 1506.05348.